Computer Modeling in Engineering & Sciences

Tech Science Press

https://doi.org/10.32604/cmes.2026.077118

ARTICLE

Adaptive Net-Profit-Based Scheduling with Minimizing Mutual Exclusion vRB Allocation in 5G-A NR Networking

Wei-Teng Chang[1] **and Ben-Jye Chang**[2,*]

[1]Graduate School of Engineering Science and Technology, National Yunlin University of Science and Technology, Yunlin, Taiwan
[2]Department of Computer Science and Information Engineering, National Yunlin University of Science and Technology, Yunlin, Taiwan

*Corresponding Author: Ben-Jye Chang. Email: benjyechang@gmail.com or changb@yuntech.edu.tw

Received: 02 December 2025; Accepted: 25 February 2026; Published: 27 April 2026

ABSTRACT: Some critical applications of emergency, Active Safe Driving (ASD), eV2X, and LEO communications require ultra-low delay and highly reliable transmission according to beyond 5G-Advanced (5G-A), 6G, and LEO specifications. Related studies proposed various scheduling algorithms in terms of single and multiple QoS requirements. However, these approaches tend to prioritize traditional QoS requirements while neglecting crucial considerations such as bearer costs and associated benefits. Moreover, most scheduling neglects the carrying cost according to the radio resource state and the bringing reward from different types of flows. Thus, this paper proposes a novel cost-based flow scheduling (eSCFS) framework that utilizes an extended sigmoid function to dynamically prioritize flows, taking into account all relevant key factors. The principal objective is to reduce latency while optimizing the utilization of radio RB and maximizing the net benefits of 5G-A NR networks. The eSCFS method has been validated through numerical simulations, which demonstrated superior key performance metrics, including network latency, resource utilization, and overall profitability. Consequently, several objectives are thus achieved: 1) analyzing the QoS requirements of various services within limited radio resources, 2) proposing a novel vRB state-dependent dynamic flow scheduling and adaptive virtual radio RB management to maximize network performance.

KEYWORDS: 5G-advanced; 6G; frequency numerology; flow scheduling; radio RB

1 Introduction

This section begins by delineating the prevailing trends and pivotal technical specifications of 5G-A/5G cellular networks. It then proceeds to examine sever related research works, including flexible frequency numerology mechanisms, BWP technology [1], and flow scheduling in 5G-A NR [2,3]. Finally, this paper investigates the pivotal challenges of RB resource allocation in 5G-A NR and provides a concise overview of the research motivations, objectives, and contributions.

1.1 5G-A/6G Network Trends and Key Standards

5G/5G-A cellular networks extensively deploy and achieve commercialization of communications for different types of flows [2–6]. Concurrently, many substantial research, technologies, and applications based on 5G, 5G-A, and 6G communications are emerging [7–10]. The key technologies involved include MEC, LEO EC [11], Vehicular/LEO Edge/5G-A EC/Cloud Computing (VEC/LEO EC/5G-A EC/VCC) [12,13], SDVN [14,15], NFV [16–18] and vRAN slicing [19–21], flow forwarding and flow steering [18], cooperative

AI networking [22], etc. MEC, LEO EC, and VEC offer a decentralized and distributed service environment characterized by lower delay and higher-speed access. By offloading computationally intensive and latency-sensitive tasks to 5G-A EC, LEO EC, or VEC servers, the execution latency of tasks is certainly reduced, and resource utilization is thus enhanced [23,24]. SDVN provides local eV2X services utilizing SDN [25] and VEC technologies, enabling flexible adaptive allocation and management of network resources. In vehicular service applications, it effectively reduces latency, enhances resource utilization, offloads computational tasks, and strengthens the QoS of eV2X applications [26]. In addition to meeting the technical capabilities discussed above, 5G-A classifies service traffic into three representative categories: uRLLC, eMBB, and mMTC. The eMBB category supports bandwidth-intensive applications, including ultra-HD media services, immersive VR/AR experiences, and cloud-assisted computing platforms. The uRLLC class targets mission-critical operations by providing extremely tighter latency bounds together with improved reliability, enabling functionalities such as Active Safe Driving (ASD), enhanced V2X communication, remote medical procedures, and emergency-response services. Meanwhile, mMTC is designed for large populations of devices, e.g., for IoT transmissions, requiring low device cost, low power consumption, low data rate, etc.

Typically, NFV is regarded as a pivotal technology for effective resource allocation in 5G/5G-A networking. Technologies such as EC, SDN, NFV, SFC [12], and Flow Steering can facilitate more efficient, flexible, and reliable network management. In 5G/5G-A, the integration of SDN, flow steering, and MEC/VCC can facilitate the realization of low-latency transmission, flexible configuration, and resource optimization. SDN enables rapid data transmission by dynamically selecting optimal paths and adapting network configurations in real-time. MEC obviously reduces transmission delay and improves response time by using the EC capabilities. AI is employed in flow steering to predictively optimize resource allocation and frequency spectrum utilization.

Furthermore, 5G/5G-A and 6G networks have the capabilities to effectively address critical issues and limitations of traditional networks, extending the fundamental functionalities of 5G-A/6G to Non-Terrestrial Networking (NTN) satellite communications. 5G-A/6G specifies urgently flowing technologies, including flow control and forwarding, collaborative artificial intelligence (AI) systems, and LEO satellite communications. These networks leverage AI and ML together with NTN LEO satellite communications. 5G-A/6G systems act as global radio access infrastructures, supporting diverse 5G-A/6G NR traffic offloading and computational operations [27]. Furthermore, for eV2X applications, AI-enabled 5G-A/6G networks can deliver the required ultra-high reliability and ultra-low latency [12,28], enhancing flow management efficiency while supporting robust communication under stringent QoS constraints.

Within the technical specifications of 3GPP Release 17, the Rel. 17-ts documents introduce mechanisms that govern the allocation of wireless RBs to satisfy a wide range of QoS KPI targets, as summarized in Table 1. In the 5G NR system, the numerology design incorporating multiple SCS configurations plays a central role in enabling these capabilities [2,3,29]. Specifically, Rel. 17-ts specifies seven SCS numerology options, denoted by $\mu \in \{0, 1, \ldots, 6\}$, where each option corresponds to a subcarrier spacing of $15\ \text{kHz} \cdot 2^{\mu}$ and an associated slot time duration of $2^{-\mu}$ (ms). Selection of an appropriate SCS is guided by the specific requirements and characteristics of each application scenario, ensuring that system performance aligns with service objectives. For instance, for mMTC applications that are not highly sensitive to latency, SCS modes $\mu = 0$ or 1 provide latencies of 2^{-0} (ms) or 2^{-1} (ms). In contrast, SCS mode $\mu = 6$ provides a minimum access latency of 2^{-6} (ms), which is well-suited for emergency communications requiring ultra-low latency.

Table 1: Key performance attributes examined for 5G, 5G-A, and 6G.

5G/B5G/6G KPIs	5G	5G-A/6G	Scenarios
Max. Frequency	90 GHz	10 THz	eMBB
Peak data rate	10 Gbps	1 Tbps	eMBB
End-to-end latency	10 ms	1 ms	Enhance uRLLC
Control Plane (CP) latency	20 ms	20 ms	Enhance uRLLC
User Plane (UP) latency	eMBB: 4 ms uRLLC: 1 ms	0.025 to 1 ms	eMBB, Enhance uRLLC
Reliability	about 99.9%	99.999%	Enhance uRLLC
Mobility	500 km/h	700 to 1000 km/h	eMBB, Mobility
Connection density	10^6 devices/km^2	107 devices/km^2	mMTC (or mIoT)
Coverage	Local coverage	Global coverage	LEO satellite

The integration of the technologies provides efficient network and resource management for 5G-A/6G, enhancing UE QoS and QoE, and satisfying the urgent QoS requirements of future mobile networks [30,31], as well as the diverse needs of various applications. The QoS KPIs for 5G-A/6G are fundamentally correspondent to those of 5G/5G-A. Table 1 provides a comparative overview of the KPIs between 5G and 5G-A/6G [30–32].

1.2 Related Studies of BWP and Frequency Numerology Key Technologies in 5G/5G-A NR

In 5G/5G-A NR networks, multiple numerology-based SCS configurations, together with configurable bandwidth parts structured under network slicing principles, have been deployed to accommodate a wide range of service requirements. This approach allows differentiated treatment for diverse traffic types, such as uRLLC and eMBB applications, while ensuring efficient utilization of radio resources. 3GPP Rel. 19 extends numerology and BWP to 5G-A and 6G [5,29]. The primary parameters of frequency numerology include the SCS in the frequency domain and the cyclic prefix length in the time domain. Different SCS modes can be chosen among $15 \cdot 2^{\mu}$ (kHz). Similarly, the selected frequency numerology determines the slot-time per subframe as $1/2^{\mu}$ (ms), with the number of slots being 2^{μ}. Parameters related to numerology SCS modes are shown in Table 2 [6,29]. Studies in [32–35] have demonstrated that utilizing flexible, different frequency numerologies brings the advantage of meeting diverse application and service requirements. Reference [32] concerns an in-depth analysis of various 5G-A NR configurations (e.g., SCS modes, MCS, scheduling methods) and traffic characteristics, bandwidth, and other system-related parameters. Reference [32] aims to perform a quantitative analysis of end-to-end latency. In [33,34], the Cost/Reward functions with static parameters are considered. Reference [35] concerns an end-to-end (E2E) latency analysis model applicable to 5G V2X scenarios. However, the disadvantages include Mutual eXclusion (MX) [36–39] in vRB allocations, where the same numerology cannot be shared simultaneously under specific SCS and slot time. Additionally, selecting different numerologies results in varying available vRB counts across SCS modes. These issues significantly reduce RB utilization in 5G, 5G-A/6G radio networks, thus impacting spectrum efficiency.

Table 2: Selected NR numerology parameters utilized by BWP.

Frequency (f)	Numerology (μ)	Time Slots (1 ms)	SCS (kHz)	Slot-Length (ms)	SC per pRB	Symbols per Slot	1 pRB (SC)	Max. pRB
	0	1	15×2^0 (15)	2^0 (1)	12	14	180 kHz	270
FR1	1	2	15×2^1 (30)	2^{-1} (0.5)	12	14	360 kHz	273
	2	4	15×2^2 (60)	2^{-2} (0.25)	12	14	720 kHz	135
	2	4	15×2^2 (60)	2^{-2} (0.25)	12	14	720 kHz	264
FR2	3	8	15×2^3 (120)	2^{-3} (0.125)	12	14	1440 kHz	264
	4	16	15×2^4 (240)	2^{-4} (0.0625)	12	14	2880 kHz	138

NR BWP based on frequency numerology is a key technology for achieving RAN slicing. BWP provides multiple independent coexistent services, each composed of several consecutive physical Resource Blocks (pRBs), as shown in Fig. 1a. NR allows three relationships between BWPs; Fig. 1b shows (Type 1) discontinuous BWP, where although NR BWPs can be discontinuous, pRBs must remain consecutive; Fig. 1c shows (Type 2) continuous BWP; and Fig. 1d shows (Type 3) multiple BWPs configured in specific frequency regions with overlapping coverage areas. It should be noted that only a single BWP can be active at any given instant. To enhance energy efficiency, reference [40] introduced a dynamic allocation mechanism that switches among different BWP sizes. In [38], two methodologies were proposed to alleviate interference caused by mixed numerology usage. Additionally, reference [39] examined the joint optimization of NR BWP configuration and SCS mode selection to improve resource utilization. In NR, the system can dynamically switch between FR1 and FR2 frequency bands, enabling data rates that are tailored to the performance requirements specified by the QoS of each traffic class.

In BWP selection [1], UEs determine which BWP set to use according to service requirements, transmitting data in either uplink or downlink. BWP switching is for UEs requiring different SCS modes. BWP switching parameters, e.g., the bwp-Inactivity Timer, among different SCS modes is set by DCI, where DCI Format 0 for UL scheduling and DCI Format 1 for DL scheduling, as well as Radio Resource Control (RRC) signaling. The primary advantage of using flexible BWP is to meet diverse application QoS. However, it definitely exhibits some disadvantages: 1) overlapping BWPs allow only one BWP to be allocated at the same time; 2) BWP switching results in mode-switching latency; and 3) reduces system throughput [7,13]. The main reason causes above disadvantages is that BWP configurations adopt a statically fixed number of consecutive pRBs (e.g., Config 1 and Config 2's RBG sizes), and thus lead to highly fragmental of available free RBs and high RB allocation failure rates.

Implementing BWP using NR numerology presents several key challenges, including: 1) addressing RB MX conflicts inherent in 5G/5G-A frequency numerology, 2) handling dynamically arriving traffic with heterogeneous flow categories that require distinct SCS numerology modes, 3) optimizing the allocation efficiency of radio RBs across multiple SCS settings, 4) effectively managing and scheduling different traffic queues, and 5) maximizing RB usage within BWP while minimizing fragmentation of contiguous available RBs.

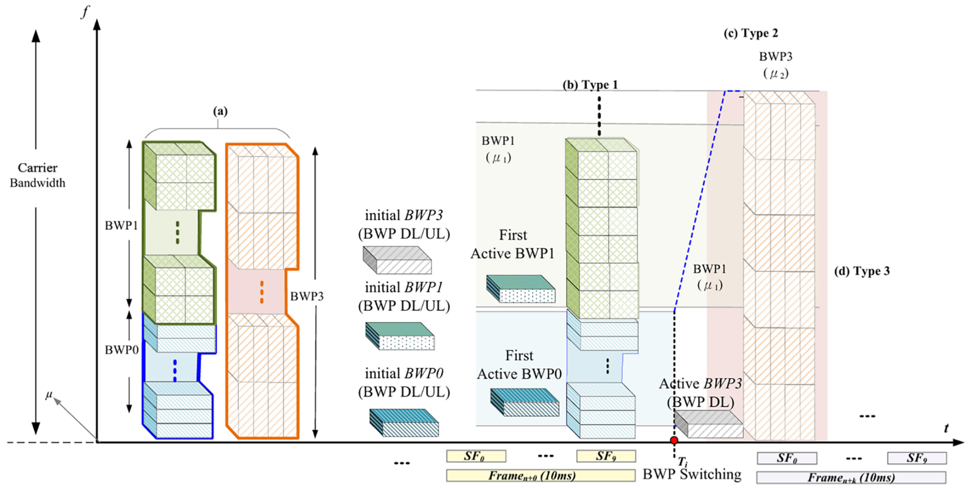

Figure 1: Illustration of BWP types and configurations in 5G-A NR as specified by 3GPP: (**a**) based on both frequency numerology and RBs considerations. (**b**) Type 1: discontinuous BWP, (**c**) Type 2: continuous BWP, and (**d**) Type 3: mixed use of different BWPs [Note that only one BWP1 (Slicing 1) or BWP3 (Slicing 3) can be used simultaneously.].

1.3 Research on Flow-Based Queueing Scheduling

In the domains of 5G-A and 6G wireless communications, the primary objective of the NR flow scheduling mechanism is to efficiently schedule and manage diverse traffic types of various application services. The core mechanism of flow scheduling is to dynamically differentiate the prioritization of flow packet processing according to single or multiple metrics, e.g., flow priority, data rate, delay, and QoS requirements of different traffic types for various applications. For instance, eMBB focuses on maximizing the utilization of wireless frequency resources. In contrast, for time-sensitive emergency communications and uRLLC applications, the emphasis is on reducing communication latency and guaranteeing high-reliability solutions. Additionally, NR flow scheduling enhances the utilization of wireless frequency resources through flexible allocation strategies. An efficient scheduling algorithm not only supports diverse application demands but also effectively guarantees radio resources to meet the QoS requirements of different flow types for various services. However, although most scheduling approaches concern multiple QoS requirements, such as packet loss, latency, and jitter, they neglect important factors: the carrying cost required by the network providers, the bringing rewards from diverse types of flows, and the optimization of radio resource utilization.

Furthermore, several representative scheduling strategies are summarized, including multi-QoS-oriented approaches (e.g., NR flexible scheduling [20]), weighted techniques (such as WFQ [41,42] and WRR [43]), priority-based methods (e.g., PQ [44,45]), and fairness-driven strategies (e.g., RR [46,47] and best channel selection [48]). While these schemes allow adaptive packet management according to single or multiple 5G-A QoS rules, they face several limitations. Typical drawbacks include: 1) challenges in simultaneously fulfilling complementary and non-complementary QoS requirements; 2) insufficient coverage of diverse flow service demands in B5G/6G networks; 3) neglect of net profit, reward, and operational cost of the network. A comparative classification and analysis of these flow scheduling strategies is provided in Table 3.

Table 3: Classification according to scheduling algorithms, performance and application.

Methods	Scheduling	Throughput	Latency	Pkt Loss	Fairness	eMergency	uRLLC	eMBB	mMTC
[20]	BWP+Slicing	✓	✓	✓			✓	✓	
[22]	BWP+DRL	✓		✓		✓	✓	✓	
[41]	EWFQ/LC		✓		✓		✓	✓	✓
[42]	Delay Weight Ratio+Priority	✓	✓				✓	✓	
[43]	WRR+Priority	✓	✓	✓			✓	✓	
[44]	Priority based	✓	✓	✓			✓		✓
[45]	Priority based		✓	✓			✓	✓	
[46]	PF+BestCQI+RR	✓	✓		✓		✓		✓
[48]	Greedy+RR	✓			✓	✓		✓	
[49]	BestCQI	✓	✓	✓			✓	✓	

1.4 Research on Flow-Based Queueing Scheduling

Several critical challenges and issues need to be efficiently addressed, as depicted below.

1. An effective adaptive scheduling method is required that simultaneously considers the fluctuating RB resource states across different frequency numerologies and meets the QoS requirements of various traffic types.
2. Research is needed on how to optimize resource allocation using the diverse characteristics of SCS modes under limited wireless RB resources to support various 5QI services.
3. An analysis based on a cost-reward algorithm is conducted to maximize the net profit and total reward of the network system while minimizing carrying costs, taking into account UE flow QoS requirements and the current RB resource states.

Thus, we propose an extended Sigmoid-based Cost-based Flow Scheduling (eSCFS) algorithm to achieve dynamic priority-based decision-making, primarily considering RB resource state in flow scheduling, extended from [33,34] with static function parameters. However, in this work, we propose the exponential-based Cost function and the adaptive Sigmoid function with dynamic parameter settings.

The main contributions include:

1. Proposing the eSCFS approach to fulfill a fully dynamic cost function and adaptive RB reward function, considering another dynamic function and dynamic MCS state.
2. Prioritizing flow packet scheduling according to the net-profit, the carrying cost (derived from the vRB state), and the bringing rewards (derived from the incoming priority of flow) in 5G/5G-A NR.
3. Maximizing RB utilization, reward, and net-profit; minimizing cost, queue delay, and flow packet loss probability.

The remainder of this paper is structured as follows. Section 2 presents the network model, detailing flow queues and wireless RB allocation across different types under 5G/5G-A NR frequency configurations. Section 3 provides a detailed description of the proposed eSCFS method, followed by numerical evaluations in Section 4. Finally, Section 5 concludes the paper and discusses potential directions for future research.

2 Network Model

First, the 5G/5G-A NR cellular communication network model based on flexible frequency numerology and BWP is described. Fig. 2 shows the 5G-A/6G NR network model for TN and NTN based on flexible

NR frequency numerology and BWP. 6G NTN-LEO networks provide edge computing and communication services in diverse scenarios, where 5G-A/6G TN experiences communication service outages and inadequate signal coverage. NR establishes various network queues to support different priority traffic k for diverse application services. The NR scheduler (e.g., RR/PF scheduler) manages the allocation and management of RB resources for different QoS-based flows. The scheduler systematically adjusts and allocates available resources based on the priority of various QoS requirements. Fig. 2 provides simple examples illustrating slicing-based end-to-end SFC flow traffic for different priority application services, depicted by dashed lines in different colors, with time-sensitive emergency flows highlighted in red. When emergency flow traffic packets reach the flow queue, they are scheduled within the 5G/5G-A gNB. Ultimately, due to the lower latency demands of emergency slices, this flow is dynamically directed to the MEC target server via SFC.

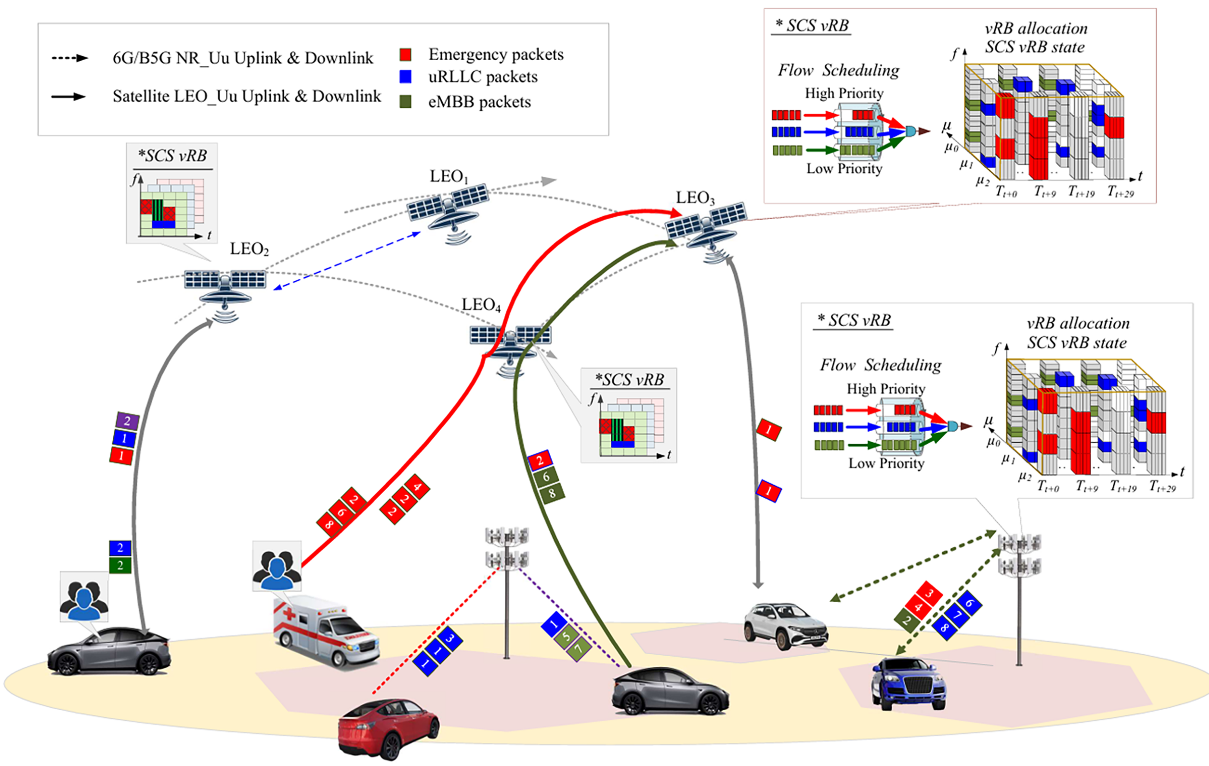

Figure 2: 5G/5G-A/6G slicing network model with flexible NR numerology, flow traffic queues, and RB resource management strategies.

This paper defines five vRB states, as shown in Table 4. The vRB states encompass available, allocated, and reserved. Additionally, there exists a blocked state arising from various μ MX responses in SCS mode under shared bandwidth policies. The pre-allocated state denotes resources that have been allocated in advance, though the corresponding flow has not yet commenced, with potential for state transition.

Table 4: Definition of vRB state indexes.

RB State	*Pre-allocated*	*Allocated*	*Available*	*Blocked*	*Reserved*
ID	2	1	0	−1	−2

Finally, the key notations employed in this paper are listed in Table 5.

Table 5: List of useful notations.

Symbol	Descriptions
BWP_μ	The BWP of type μ flow
C_μ	The function of the cost
$\mathbb{N}^{OPT}$	Flow queue of type μ with highest positive net profit for scheduling
$QS_{\mu,k}$	A UE with priority class k utilizing SCS mode μ in the scheduling process of its flow queue.
U_μ	Number of occupied vRBs (allocated or blocked)
d_μ	The μ flow type delay boundary
$\triangle f_{\mu,vrb}$	The bandwidth of an RB
$k = 1, 2, \ldots K$	Traffic flow class k, with $k = 1$ highest and $k = K$ lowest priority.
q_μ	Total available RBs for μ-type flow within its delay constraint.
$sf^{id}_{\mu,vrb}$	The vRB's designated subcarrier position in frequency.
$sf^{id}_{\mu,prb}$	The pRB's assigned subcarrier location in the spectrum.
T	Duration of the physical-layer frame.
$ts^{id}_{\mu,t}$	Slot-level temporal index.
t	The slot index corresponding to a specific subframe. (time slot)
$t_{i\rightarrow i+r}$	Time interval from t to $t + r$
$vRB^{state}_{\mu,tf,ts,k}$	State of vRB in SCS mode μ at slot ts and sub-carrier sf for μ-type flow
vRB^{ID}_μ	vRB Index (ID) for type μ flow
$\Gamma_{\mu,i,k}(\cdot)$	Reward function for a priority UE in SCS mode μ
Φ_μ	Parameter for vertical rate of change in the reward curve
α, β	Pareto distribution parameters for traffic generation
μ	SCS mode representing frequency numerology
δ_μ	The gradient rate of type μ flow
η_μ	Weighting factor of type μ flow
ρ_μ	Turning point of type μ flow
ω_μ	PI for the flow μ type

3 The Proposed eSCFS Approach

This section depicts the proposed dynamic flow scheduling solution implemented in a virtualized 5G-A/6G NR and the eSCFS, as shown in Fig. 3. This approach efficiently addresses the 3GPP static and pre-configured RB allocation specification, and achieves the optimization for flow scheduling and wireless RB resource allocation in 5G-A/5G NR. This requires maximizing the utilization of radio bearers (RBs) and minimizing delays and loss opportunities for flows with the highest priority traffic. It is worth noting that the eSCFS method considers the RB status of radio resources, thereby facilitating the dynamic allocation of flow scheduling priorities.

Through the eSCFS method, the uplink incoming queue receives different types of data packets from various UEs in 5G-A NR. Subsequently, NR determines the processing order of data packets based on the specific 5-tuple flow ID (i.e., L3 IP addresses and L4 Transport ports of source and destination, respectively, and Flow Type). The eSCFS approach prioritizes packets with the highest net-benefit.

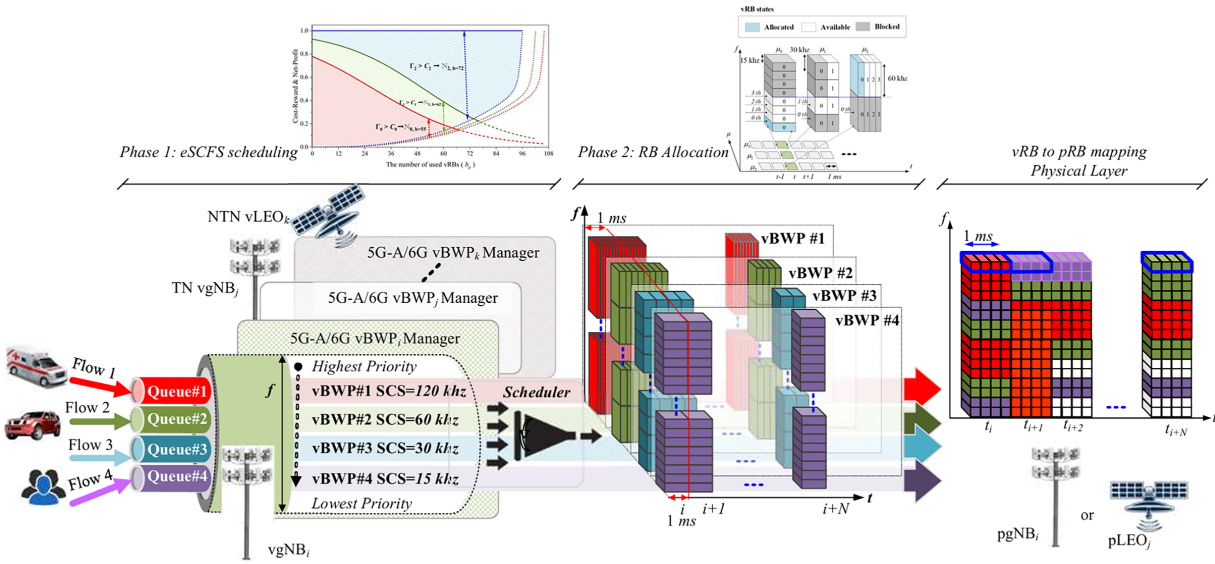

Figure 3: The approach model of the proposed eSCFS for the 5G/5G-A NR.

3.1 Optimal Problem Definition and Constraints

Initially, to achieve the proposed net-profit-based scheduling algorithm for multiple-queue for different types of flows in 5G-A, we define the scheduling algorithm as an optimal problem, in which the scheduler determines and schedules the flow packet of the Head of Line (HoL) of a flow queue that results in the largest net-profit. At the same time, for guaranteeing the QoS of flow packets according to the required QoS KPI specified in 3GPP 5G-A [30] for diverse types of flows. Several QoS constraints are limited, including maximum packet delay (denoted as $d_{\mu,\max}$), maximum packet loss probability (denoted as $p_{\mu,\max}^{loss}$), minimum, average, and maximum data rate (denoted as $r_{\mu,\max}$, $r_{\mu,\text{avg}}$ and $r_{\mu,\min}$), the carrying cost (C_{μ}^{HoL}) and the bringing reward (Γ_{μ}^{HoL}). As a result, the optimal problem for the net-profit scheduling algorithm is defined as follows.

$$Packet_{\mu}^{*} \leftarrow \arg\max_{\forall\mu}\left\{B_{\mu}^{HoL} = \Gamma_{\mu}^{HoL} - C_{\mu}^{HoL}\right\}, \tag{1}$$

s.t.,

$$\begin{aligned}
&\text{C1: } A_{k,\mu,m} = \begin{cases} 1,\ \text{if}\left(d_{\mu,m}^{HoL} \le d_{\mu,\max} \&\& p_{\mu,m}^{HoL,loss} \le p_{\mu,\max}^{loss} \&\& q_{\mu}^{vRB} > b_{\mu}^{HoL,vRB}\right) \\ 0,\ \text{else if}\left(d_{\mu,m}^{HoL} > d_{\mu,\max} \| p_{\mu,m}^{HoL,loss} > p_{\mu,\max}^{loss}\right) \end{cases} \\
&\text{C2: } \Gamma_{\mu}^{HoL} > C_{\mu}^{HoL} \text{ and } \Gamma_{\mu}^{HoL} - C_{\mu}^{HoL} > 0 \\
&\text{C3: } 0.0 \le C_{\mu}^{HoL} \le 1.0 \\
&\text{C4: } 0.0 \le \Gamma_{\mu}^{HoL} \le 1.0.
\end{aligned} \tag{2}$$

In Eq. (2), for *Constraint 1* (***C1***), for the HoL packet (originating from UE m) of type μ flow queue, if the delay ($d_{\mu,m}^{HoL}$) is less than the maximum KPI packet delay ($d_{\mu,\max}$); the loss probability ($p_{\mu,m}^{HoL,loss}$) is less than the maximum KPI packet loss probability ($p_{\mu,\max}^{loss}$); and the vRB state ($b_{\mu}^{HoL,vRB}$) is smaller than the total vRB capacity (q_{μ}^{vRB}), $A_{\mu,m}$ is set to 1 (i.e., the HoL packet satisfies the required QoS constraints of ***C1***). Otherwise, $A_{\mu,m}$ is set to 0.

For *Constraint 2* (***C2***), the bringing reward (Γ_{μ}^{HoL}) of the corresponding HoL packet should exceed the carrying cost (C_{μ}^{HoL}) and the net-profit should be positive (i.e., $\Gamma_{\mu}^{HoL} - C_{\mu}^{HoL} > 0$). For *Constraint 3* (***C3***), the value of the carrying cost (C_{μ}^{HoL}) should range to [0, 1]. For *Constraint 4* (***C4***), the value of the bringing reward (Γ_{μ}^{HoL}) should range to [0, 1].

3.2 Dynamic Exponential Cost Function, $C_{\mu}(\cdot)$

In the extant literature on flow queue scheduling, authors consistently prioritize developing scheduling solutions tailored to specific performance indicators, such as maximizing data rate and reliability, and minimizing delay and loss, while largely overlooking the status of radio RB resources. To facilitate subsequent processing and transmission, this article proposes the utilization of an exponential cost function, which is predominantly employed for determining carrying costs. This function primarily considers two pivotal parameters: 1) Based on frequency numerology, the total number of vRBs of each type μ flow within the delay bound condition, represented by q_{μ}, and 2) In the resource-sharing environment, calculating the total number of vRB resource states of each type μ flow comprising allocated and blocked states only, represented by b_{μ}. Eq. (3) presents the formulation of the cost function $C_{\mu}\left(q_{\mu}, b_{\mu}\right)$, which is based on an exponential model.

$$C_{\mu}\left(q_{\mu}, b_{\mu}\right) = 2^{n} \cdot \left(q_{\mu}^{-e} \cdot b_{\mu}^{e} + \eta_{\mu}\right), \tag{3}$$

where

$$\eta_{\mu}\left(q_{\mu}, b_{\mu}\right) = \left(2^{n} \cdot \left(q_{\mu} - b_{\mu}\right) \cdot \left(q_{\mu} - b_{\mu} + 1\right) + 1\right)^{-1}$$
$$subject\ to\ 0 < \eta_{\mu} \leq 1 \tag{4}$$

In Eqs. (3) and (4), n ($n \leq 0$) denotes the shrink exponent factor and η_{μ} is a dynamic fine-tuning weighting factor used to adjust the number of available RBs.

Obviously, as the dynamic fine-tuning factor of η_{μ} increases, the number of available vRBs decreases, leading to a significant increase in the carrying cost $C_{\mu}(\cdot)$, and *vice versa*. For vRB resources in the individual type μ flow, as the number of allocated (or used) resources increases, the carrying cost increases exponentially. Note that due to differences in available RB resources between different SCS modes in numerology, the number of available vRB resources varies across different flow types μ. Specifically, within a 20 MHz frequency band, three distinct numerology SCS modes (i.e., $\mu = 0, 1, 2$) within each 1 ms sub-frame, the maximum number of RBs available for each mode is: 106 (106 * 1) RBs for μ_0, 102 (51 * 2) RBs for μ_1, and 96 (24 * 4) RBs for μ_2. Due to the constraints imposed by delay bounds (specifically, 50 ms for μ_0, 10 ms for μ_1 and 5 ms for μ_2), the upper-bound RBs for various flow types μ extend to 5300 (106 * 50) RBs for μ_0, 1020 (102 * 10) RBs for μ_1, and 480 (96 * 5) RBs for μ_2. In a single SCS mode, the impact of variations in the number of RBs utilized on the associated cost is clearly observable, reflecting the sensitivity of the system performance to resource allocation.

Specifically, the cost reaches its peak value of 1.0 when all available RBs are employed, indicating the maximum resource utilization scenario, whereas it falls to its minimum value of 0.0 when no RBs are consumed, corresponding to the idle allocation condition. Then, a numerical example of three vRB states is presented in detail to demonstrate the determined cost values. From these numerical examples, the maximum and minimum cost values can certainly justify the bounds (i.e., the cost is 0.0 if the vRB state is fully occupied; conversely, the cost is 1.0 if the vRB state is totally free) of the proposed cost function. Consequently, by leveraging the exponential cost function, eSCFS systematically evaluates the state of each vRB, thereby facilitating informed and adaptive scheduling decisions that dynamically respond to the current resource availability and service requirements.

Assume that the 5G-A gNB adopts a 20 MHz frequency spectrum bandwidth and a 5 ms delay bound of SCS mode μ_2 vRB (i.e., with the total number of vRBs is $q_2 = 480$, $24\,(\text{RBs/time\_slot}) \cdot 4\,(\text{time\_slot/subframe}) \cdot 5\,(\text{ms/1slot}) = 480$) for three vRBs states of 1) $b_2 = 0$ (all vRBs are free) in Scenarios 1 and 2) $b_2 = 220$ in Cases 2 and 3) $b_2 = 480$ (i.e., all vRBs are occupied) in Scenario 3.

Scenario 1. For type μ_2 flow with vRB state $b_2 = 0$, calculate the dynamic fine-tuning weighting factor $\eta_2\,(480, 0)$ and the carrying cost $C_2\,(480, 0)$.

$$\eta_2\,(480, 0) \leftarrow \left(0.5 \cdot (480 - 0) \cdot (480 - 0 + 1) + 1\right)^{-1} = 8.6624\text{E} - 07$$
$$C_2\,(480, 0) \leftarrow 0.5 \cdot \left(480^{-e} \cdot 0^{e} + \eta_2\,(480, 0)\right) = 4.33\text{E} - 06$$

Scenario 2. For type μ_2 flow with vRB state $b_2 = 220$, calculate the dynamic fine-tuning weighting factor $\eta_2\,(480, 220)$ and the carrying cost $C_2\,(480, 220)$.

$$\eta_2\,(480, 220) \leftarrow \left(0.5 \cdot (480 - 220) \cdot (480 - 220 + 1) + 1\right)^{-1} = 2.94716\text{E} - 05$$
$$C_2\,(480, 220) \leftarrow 0.5 \cdot \left(480^{-e} \cdot 220^{e} + \eta_2\,(480, 220)\right) = 0.059989$$

Scenario 3. For type μ_2 flow with vRB state $b_2 = 480$, calculate the dynamic fine-tuning weighting factor $\eta_2\,(480, 480)$ and the carrying cost $C_2\,(480, 480)$.

$$\eta_2\,(480, 480) \leftarrow \left(0.5 \cdot (480 - 480) \cdot (480 - 480 + 1) + 1\right)^{-1} = 1$$
$$C_2\,(480, 480) \leftarrow 0.5 \cdot \left(480^{-e} \cdot 480^{e} + \eta_2\,(480, 480)\right) = 1$$

3.3 Extended Sigmoid-Based Reward Function, $\Gamma_\mu\,(\cdot)$

Furthermore, eSCFS proposes an enhanced Sigmoid dynamic reward function to explicitly identify rewards generated by packets from incoming flows. Key features of the eSCFS reward function include the ability for the reward curve to dynamically adjust horizontally, vertically, and diagonally effectively. According to the proposed cost–reward-driven scheduling algorithm, the flow packet exhibiting the highest net profit is designated the most prioritized for scheduling. Two primary aims can be accomplished. Firstly, it offers a dynamic scheduling approach that considers numerous variables, including MCS (such as calculation order parameters), frequency numerology, and RB status. Secondly, the flow packet with the greatest net profit is given the highest priority, and the queue scheduler processes it first. Prioritizing the highest priority provides a range of advantages, including minimizing network costs and maximizing the system's net profit and reward.

eSCFS examines the conventional sigmoid function defined in Eq. (5) and its alignment with the characteristic S-shaped transition, highlighting two principal elements: the natural base e (Euler's number) that structures the exponential term, and a shaping parameter whose evolution exhibits a transition pattern reminiscent of the error function.

$$f\,(t) = 1/\left(1 + e^{-t}\right). \tag{5}$$

In Eq. (5), the Sigmoid-based formulation depicts a dynamic growth pattern characterized by an inflection point. Prior to this point, the formulation demonstrates exponential growth, suggesting a gradient rate that is higher than but smaller than the inflection point value. Conversely, after this point, logarithmic growth is evident, with a gradient rate that is lower in the interval before the inflection point but greater than the inflection point value. As illustrated in Eq. (6), the enhanced sigmoid-based adaptive reward function

$\Gamma_\mu(\cdot)$ is introduced by eSCFS through the utilization of the maximum value of Sigmond's S-shaped curve, based on the integration of several significant parameters, represented by Γ_μ.

1. ρ_μ denotes the impact factor of pivot ρ_μ affecting the turning point P_μ of the reward function curve. That is, the pivot turning point P_μ moves toward the left, while ρ_μ increasing, and *vice versa*.
2. δ_μ denotes the impact factor of slope δ_μ affecting the S-shaping of the reward function curve (of the extended Sigmoid function). That is, the S-shaping of the reward function curve becomes sharp, while δ_μ increasing, and *vice versa*.
3. ϑ_{μ,i,Q_m} denotes the weighting factor according to the MCS. ϑ_{μ,i,Q_m} decreases, as the MCS Q_m increasing.
4. Φ_μ denotes the peak parameter of the maximum reward for flow type μ, and
5. ω_μ denotes the factor for the fine-tuning of the rate of inflation.

$$\Gamma_{\mu,i,k} \leftarrow \left(1+\left(e^{-\delta_\mu\cdot\left(\left(q_\mu-b_\mu\right)-\rho_\mu\right)}\right)\right)^{-\Phi_{\mu,i}} + \omega_\mu, \text{s.t.}\delta_\mu \geq 0, \Phi_\mu \geq 0. \tag{6}$$

The control parameter ρ_μ is inversely proportional to the turning point P_μ. When $\rho_\mu \leq 0$, it indicates that all resources can be utilized, and P_μ is close to the maximum vRB usage, as depicted by the S6 curve in Fig. 4. As ρ_μ increases, the available vRBs decrease. When ρ_μ approaches the maximum value of vRBs used, there are nearly no resources available. At this stage, P_μ will be close to or lower than the minimum vRB usage value, as illustrated by the S7 curve in Fig. 4.

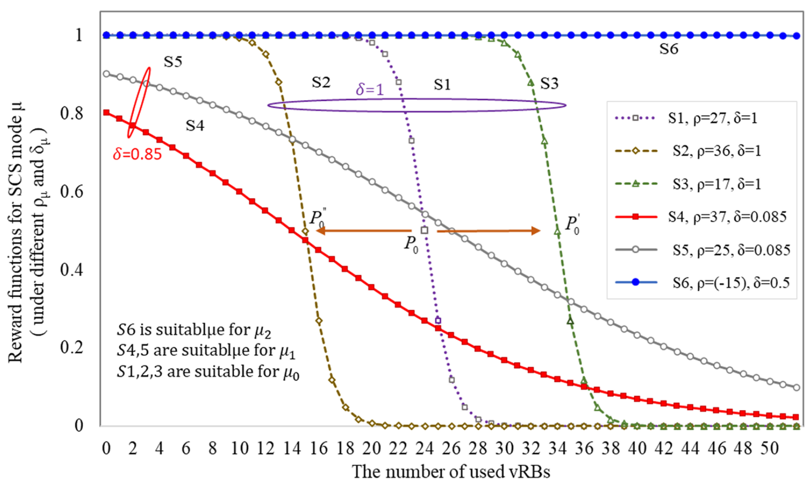

Figure 4: Reward functions for SCS mode $\mu = 0$ (under different ρ_μ and δ_μ).

Further analysis of the adaptive turning point P_μ in the reward function is conducted according to flow type μ. The primary objective is to determine the correlation between the reward value at the turning point and vRB utilization. The turning point P_μ is positioned near the maximum number of vRBs, resulting in higher rewards, which is suitable for higher priority flow types. Conversely, for lower priority flow types, the turning point P_μ should be closer to the minimum, resulting in lower rewards. It is important that the inflection point is adaptively adjusted according to the vRB state.

Third, the behavior of the reward function near its transition point is characterized by analyzing its local gradient. The principal purpose of slope rate δ_μ is to ascertain the rate of change in reward value between the maximum of 1.0 and the minimum of 0.0, as shown in Fig. 4. As the slope rate δ_μ approaches 1.0, the shape of the function becomes increasingly sharp, as curves S1, S2, and S3 are illustrated in Fig. 4. Conversely, as the slope rate δ_μ approaches 0.0, the reward function becomes increasingly smooth, as curves S4, S5, and S7 illustrated in Fig. 4. Importantly, when the slope rate δ_μ is equal to zero, the reward formula curve becomes horizontal, as curve S8 illustrated in Fig. 4. In consequence, for higher traffic rates, a greater slope rate δ_μ is needed under higher vRB states, thereby facilitating the acquisition of more substantial rewards, as curve S6 illustrated in Fig. 4. In contrast, a smaller slope rate δ_μ is better suited for lower traffic types. It allows for a more limited set of vRB states to be covered, resulting in the possibility of achieving greater rewards, as curve S2 demonstrated in Fig. 4. By adjusting slope rate δ_μ for different types of traffic, it dynamically optimizes the bringing reward formula.

Next, we analyze the variation of the peak value of the maximum reward in the reward function between its maximum and minimum values. The peak value $\Phi_{\mu,i,m}$ primarily induces significant variation in the maximum and minimum reward values for different priorities of flows. The parameter formula for the peak value is formulated in Eq. (7).

$$\Phi_{\mu,i,m} = \left(e^{-\vartheta_{\mu,i,Q_m}}\right)^{(\mu_{\max}-\mu_k)}, \tag{7}$$

where i denotes the i-th UE, μ_k denotes the numerology SCS mode for type k flow and ϑ_{μ,i,Q_m} is a weighting factor according to the MCS Q_m. Moreover, in 5G-A TN or further 6G NTN, the MCS Q_m of an UE definitely affects the number of required vRBs and the bringing reward.

The weighting factor ϑ_{μ,i,Q_m} according to MCS Q_m is formulated in Eq. (8).

$$\vartheta_{\mu,i,Q_m} \leftarrow \left(Q_m^{\max} - Q_{m,i,\mu_k} + 1\right) / \left(Q_m^{\max} + Q_m^{\min}\right), \tag{8}$$

where $Q_m^{\max}$ and $Q_m^{\min}$ denote the maximum and minimum values of the modulation order (i.e., Q_m), respectively. For instance, $Q_{256qam} = 8$ denotes the maximum MCS of 256 QAM for, $Q_{16qam} = 4$ for 16 QAM and $Q_{qpsk} = 2$ for QPSK. In addition, $Q_{m,i,\mu}$ denotes MCS Q_m with SCS mode μ, where $\mu_{\max}$ denotes the maximum SCS mode. For example, for three types of flows μ, $\mu \in \{0,1,2\}$, $\mu_{\max} = 2$ and $\mu_{\min} = 0$.

In summary, the analyses and discussions of the key impact factors of the reward function are depicted as follows, including the total number of vRBs q_μ, the vRB state of allocated and blocked b_μ, the impact factor of pivot ρ_μ affecting the turning point P_μ of the reward function curve, the impact factor of slope δ_μ affecting the S-shaping of the reward function curve, the MCS Q_m, the weighting factor according to the MCS ϑ_{μ,i,Q_m}, and the peak value of maximum reward $\Phi_{\mu,i,m}$. Consequently, from Eq. (6), the reward function of $\Gamma_{\mu,i,k} \leftarrow \left(1 + \left(e^{-\delta_\mu \cdot ((q_\mu - b_\mu) - \rho_\mu)}\right)\right)^{-\Phi_{\mu,i}} + \omega_\mu$ exhibits several features.

Feature 1: The impact factor of pivot ρ_μ affects the turning point P_μ of the reward function curve. That is, the pivot turning point P_μ moves toward the left, while ρ_μ increasing, and *vice versa*.

Feature 2: The impact factor of slope δ_μ affects the S-shaping of the reward function curve (of the extended Sigmoid function). That is, the S-shaping of the reward function curve becomes sharp, while δ_μ increasing, and *vice versa*.

Feature 3: For the residual available RBs $\left(q_\mu - b_\mu\right)$, the bringing reward increases, while the available RBs $\left(q_\mu - b_\mu\right)$ decreasing.

Feature 4: The weighting factor according to the MCS ϑ_{μ,i,Q_m} decreases, as the MCS Q_m increasing. (i.e., ϑ_{μ,i,Q_m} is inversely proportional to Q_m)

Feature 5: The peak value of maximum reward $\Phi_{\mu,i,m}$ increases, as the weighting factor ϑ_{μ,i,Q_m} decreasing. (i.e., $\Phi_{\mu,i,m}$ is inversely proportional to ϑ_{μ,i,Q_m})

Feature 6: The bringing reward $\Gamma_{\mu,i,k}$ increases, as the peak value of maximum reward $\Phi_{\mu,i,m}$ increasing. (i.e., $\Gamma_{\mu,i,k}$ is proportional to $\Phi_{\mu,i,m}$)

Specifically, $\Phi_{\mu,i,m}$ is inversely proportional to $\vartheta_{\mu,i,\mathrm{Q}_m}$. Thus, a larger MCS Q_m (e.g., $Q_{256qam} = 8$) yields lower $\vartheta_{\mu,i,\mathrm{Q}_m}$ and higher $\Phi_{\mu,i,m}$. Furthermore, Φ_μ is directly proportional to SCS mode μ, so a higher μ (e.g., μ_2) yields a higher $\Phi_{\mu,i,m}$.

For clearly demonstrating how to determine the dynamic reward function, as shown in Eqs. (7) and (8), three numerical examples for three scenarios using different SCS modes provide clear intuition on the determinations of the bringing reward, respectively. Assume that UE_i with three types of flows of eMergency, uRLLC, and eMBB, using three SCS modes $\mu \in \{0, 1, 2\}$ and different MCS of $Q_{256qam} = 8$ and $Q_{16qam} = 4$, etc., $\vartheta_{8,i,2}$ and $\Phi_{8,i,2}$ for UE_i are determined below, respectively.

Scenario 1. For type μ_2 flow using either $Q_{256qam} = 8$ or $Q_{16qam} = 4$, calculate $\vartheta_{8,i,2}$ and $\Phi_{8,i,2}$ for UE_i,

$$\vartheta_2 \leftarrow \begin{cases} \vartheta_{8,i,2} = \left((8-8+1)/(8+2)\right)_i = 0.1 \text{//higher MCS} \\ \vartheta_{4,i,2} = \left((8-4+1)/(8+2)\right)_i = 0.5 \end{cases}$$

$$\Phi_2 \leftarrow \begin{cases} \Phi_{8,i,2} = \left(e^{-0.1}\right)^{(2-2)} = 1 \\ \Phi_{4,i,2} = \left(e^{-0.5}\right)^{(2-2)} = 1 \end{cases}$$

Scenario 2. For type μ_1 flow using either $Q_{256qam} = 8$ or $Q_{16qam} = 4$, calculate $\vartheta_{8,i,1}$ and $\Phi_{8,i,1}$ for UE_i,

$$\vartheta_1 \leftarrow \begin{cases} \vartheta_{8,i,1} = \left((8-8+1)/(8+2)\right)_i = 0.1 \text{//higher MCS} \\ \vartheta_{4,i,1} = \left((8-4+1)/(8+2)\right)_i = 0.5 \end{cases}$$

$$\Phi_1 \leftarrow \begin{cases} \Phi_{8,i,1} = \left(e^{-0.1}\right)^{(2-1)} = 0.9048 \text{//better} \\ \Phi_{4,i,1} = \left(e^{-0.5}\right)^{(2-1)} = 0.6065 \end{cases}$$

Scenario 3. For type μ_0 flow using either $Q_{256qam} = 8$ or $Q_{16qam} = 4$, calculate $\vartheta_{8,i,0}$ and $\Phi_{8,i,0}$ for UE_i,

$$\vartheta_0 \leftarrow \begin{cases} \vartheta_{8,i,0} = \left((8-8+1)/(8+2)\right)_i = 0.1 \text{//higher MCS} \\ \vartheta_{4,i,0} = \left((8-4+1)/(8+2)\right)_i = 0.5 \end{cases}$$

$$\Phi_0 \leftarrow \begin{cases} \Phi_{8,i,0} = \left(e^{-0.1}\right)^{(2-0)} = 0.8187 \text{//better} \\ \Phi_{4,i,0} = \left(e^{-0.5}\right)^{(2-0)} = 0.3679 \end{cases}$$

From the above justifications and discussions of these three scenarios, we can conclude that a higher MCS Q_m (e.g., $Q_{256qam} = 8$) can achieve a lower weighting factor $\vartheta_{\mu,i,\mathrm{Q}_m}$, a higher peak value $\Phi_{\mu,i,m}$, and a higher bringing reward $\Gamma_{\mu,i,k}$, and *vice versa*.

Fig. 5 depicts the reward function curves under different peak values $\Phi_{\mu,i,m}$, where δ and ρ are set to 240 and 0.02, respectively. $\Phi_{\mu,i,m}$ varies from 0.2 to 1.0. Obviously, the maximum reward value increases (e.g., S5 curve of the reward function), as the peak value parameter $\Phi_{\mu,i,m}$ increasing (e.g., $\Phi_{\mu,i,m} = 1.0$). Note that the highest reward function of S5 is suitable for the highest flow type μ_2; conversely, the lowest reward function S1 is for the lowest flow type μ_0.

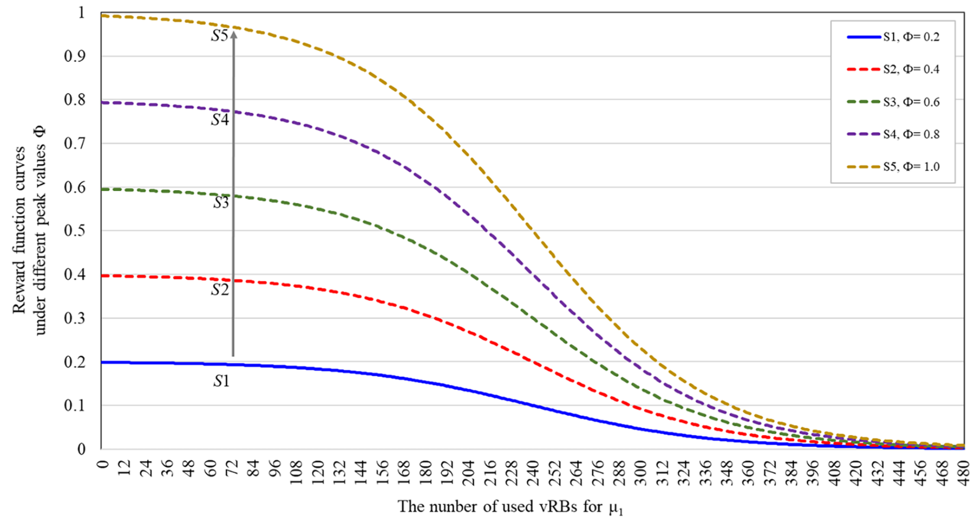

Figure 5: Different reward function curves of different peak values $\Phi_{\mu,i,m}$ under different vRB states (for $\mu = 1$, $\rho = 240$, $\delta = 0.02$).

3.4 Scheduling the Flow Packet with the Highest Net-Profit

As shown in Fig. 6, the benefit models associated with each flow category are generated in a manner that incorporates their corresponding dynamic parameters. Following the formulation of the exponential cost expression and the enhanced sigmoid-based benefit model, the eSCFS scheduler selects, from the queue, the packet whose net gain is strictly positive and numerically the largest. This packet is treated as the scheduling winner, represented by $\mathbb{N}_{\mu*}^{OPT}$, and follows the definition given in Eq. (9).

$$\mathbb{N}_{\mu*}^{OPT} \leftarrow \arg\max_{\forall\mu} \left\{\Gamma_\mu - C_\mu\right\}. \tag{9}$$

As shown in Fig. 6 and Eq. (9), only the flow packets for which the bringing reward exceeds the associated carrying cost, i.e., $\Gamma_\mu > C_\mu$, are considered candidates for scheduling. Subsequently, among these flow HoL packets of all flow queues, the net-profit scheduling algorithm selects the HoL packet with maximum net-profit as the optimal one to be scheduled to the next stage of vRB allocation.

Consequently, the eSCFS scheduling algorithm exhibits several distinctive advantages, particularly in comparison to existing scheduling methods. First, a flow packet is only eligible for scheduling if its reward exceeds the carrying cost, expressed as $\Gamma_\mu > C_\mu$. Second, the eSCFS scheduling strategy is designed to optimize the network's net profit. Packets with the highest positive net profit are prioritized for scheduling, while ensuring compliance with various QoS parameters. Moreover, the scheduling process incorporates multiple dynamic factors associated with the states of both the flow queue and the virtual RBs (vRBs), enhancing overall scheduling efficiency. Certainly, the determination of the optimization scheduling result benefits from the above proposed dynamic states of flow queue, vRB state, and important parameters.

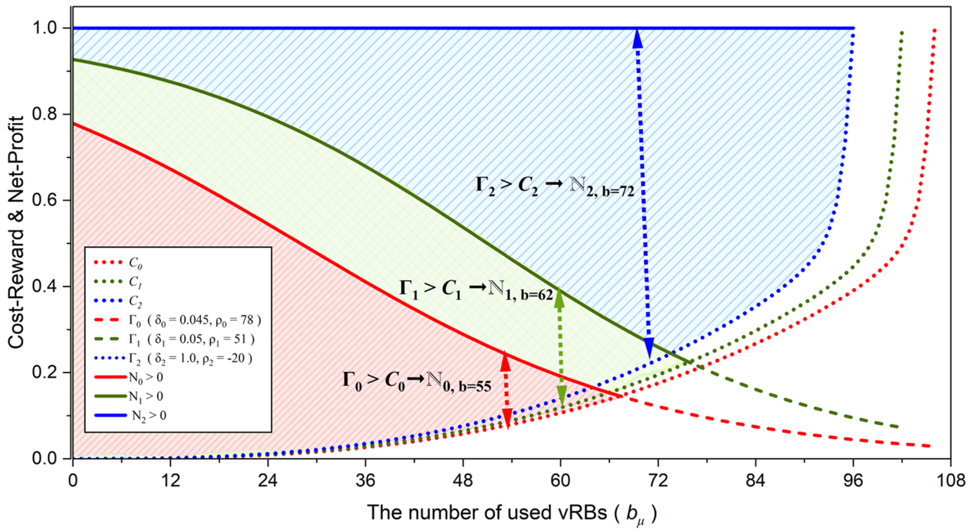

Figure 6: Extended sigmoid reward function, exponential-based cost function, and the net-profit of different SCS modes under various vRB states.

In summary, specifically, for the proposed exponential Cost Function, the cost function is formulated based on the dynamic parameters, including: 1) the dynamic vRB state b_μ, 2) the total number of vRBs within the delay bound of the corresponding SCS mode μ, and 3) a dynamic fine-tune up factor η_μ. Typically, the total number of vRB resource states, b_μ, of each type μ flow consists of the number of allocated and blocked states. η_μ denoting the fine-tuning weighting factor, is to adjust the number of available RBs. Obviously, as the fine-tuning of η_μ increases, the number of available vRBs decreases, resulting in a significant increase in the carrying cost $C_\mu(\cdot)$, and *vice versa*. For the proposed adaptive Reward function, the reward function, $\Gamma_{\mu,i,k} \leftarrow \left(1 + \left(e^{-\delta_\mu \cdot ((q_\mu - b_\mu) - \rho_\mu)}\right)\right)^{-\Phi_{\mu,i}} + \omega_\mu$, is formulated as an efficient Adaptive-Sigmoid function with some dynamic parameters and an adaptive function, $\Phi_{\mu,i,} = \left(e^{-\vartheta_{\mu,i,Q_m}}\right)^{(\mu_{\max} - \mu_k)}$, according to the MCS states (i.e., 256QAM, 64QAM, 16QAM, etc.) of the concerned UE.

Finally, the algorithm of the proposed eSCFS scheduling and vRB allocation is shown in Algorithm 1.

Algorithm 1: eSCFS scheduling & vRB allocation

Definitions:

$vQ = \{vq_2, vq_{1,}, vq_{0,}\}$: Set of virtual queues corresponding to numerology types.
d_μ: Delay bound of SCS mode μ.
q_μ: Total number of vRBs within the delay bound d_μ for SCS mode μ.
b_μ: Number of occupied vRBs (Allocated + Blocked) of SCS mode μ.
$\mathrm{T}_\mu(t)$: Set of vRB candidates of SCS mode μ at scheduling instant time t.
$C_\mu(q_\mu, b_\mu)$: Cost function.
$\Gamma_\mu(\cdot)$: Reward function.

Inputs:

$vQ \leftarrow 3$, q_μ, b_μ, d_μ, $\mathrm{T}_\mu(t)$, C_μ, $\Gamma_{\mu,i,k}$, $\mathbb{N}_\mu$, Parameters $\{\delta_\mu, \vartheta_\mu, \omega_\mu \leftarrow 0\}$

Outputs:

– Optimize vRB allocation for the optimal flow packet de-queued by the scheduler.

(Continued)

Algorithm 1 (continued)

– Update vRB states $s\left(vrb_{\mu,j}\right) \in \{Free\ (0), Allocated\ (1), Blocked\ (-1)\}$.
– Update the occupied vRBs b_μ and residual vRBs l_μ.
– Drop flow packet if no feasible vRB can be allocated within the delay bound.

Initialize vRB state $s\left(vrb_{\mu,j}\right) \leftarrow$ Free (0), $\forall vrb_{\mu,j} \in vRB_\mu$, $\forall \mu \in \{2,1,0\}$, $b_\mu \leftarrow 0$,
Generate $|u|$ UEs and initialize traffic flows
while (Current_time < Simulation_time) do
    /** Phase 1: Net-Profit-Based HoL Flow Scheduling **/
    for each $vq_\mu \in vQ$ do
        if vq_μ is empty then
            $\mathbb{N}_\mu \leftarrow -\infty$
            continue
        end if
        // Update vRB state
        b_μ ← Number of vRBs with states {Allocated, Blocked} in vRB_μ
        $l_\mu \leftarrow q_\mu - b_\mu$
        Let i be the HoL packet in vq_μ
        Update waiting time $w_{\mu,i}(t)$
        //Cost must be computed after b_μ is updated
        Compute cost $C_\mu\left(q_\mu, b_\mu\right)$
        //Randomly generate flow packet quality FQ_μ
        from $MCS = \{1,2,6,8\}$,
        with $P\left(FQ_\mu = MCS\right) = \begin{cases} \frac{1}{4}, h \in MCS \\ 0, otherwise \end{cases}$
        Update ϑ_μ using Eq. (8)
        Compute $\Phi_{\mu,i}$ using Eq. (7)
        Compute reward $\Gamma_{\mu,i,k}$ using Eq. (6)
        $\mathbb{N}_\mu \leftarrow \Gamma_{\mu,i,k} - C_\mu\left(q_\mu, b_\mu\right)$
    end for
    if $\mathbb{N}_\mu^* \leq 0$ then
        break
    end if
        //Select candidate queue:
        $\mathbb{N}_{\mu*}^{OPT} \leftarrow \arg\max_{\forall \mu} \{\Gamma_\mu - C_\mu\}$. using Eq. (9)
    Dequeue the optimal HoL packet i^* from vq_μ^*
    /** Phase 2. RB Allocation **/
    $Flag\_success \leftarrow false$
    for each slot-time $t_j \in T_{\mu^*}(t)$ do
        if $w_{\mu^*,i^*}(t) + t_j \leq d_{\mu^*}$ then
            if $s\left(vrb_{\mu,j}\right) == Free$ && $b_{\mu^*} < q_{\mu^*}$ then //Optimal vRB for allocation
                // Allocate $vrb_{\mu,j}$ to flow i*:
                $s\left(vrb_{\mu,j}\right) \leftarrow Allocated\ (1)$
                $b_{\mu^*} \leftarrow b_{\mu^*} + 1$

(Continued)

Algorithm 1 (continued)

$l_{\mu^*} \leftarrow q_{\mu^*} - b_{\mu^*}$
//Block overlapped vRBs:
for each $v \in \{2, 1, 0\}, v \neq \mu^*$ do
  if $s\left(vrb_{\mu,j}\right) == Free\,(0)$ then
    $s\left(vrb_{\mu,j}\right) \leftarrow Blocked\,(-1)$
    $b_v \leftarrow b_v + 1$
    $l_v \leftarrow q_v - b_v$
  end if
end for
$Flag\_success \leftarrow true$
break
end if
end if
end for
if $Flag\_success == false$ then
Delete (dropping) packet i^*
end if
end while

4 Numerical Results

This section presents an evaluation and comparison of key performance metrics for the proposed eSCFS approach and several related methods, as summarized in Table 6. The benchmarked approaches include the 3GPP 5G/5G-A NR radio resource allocation specification (denoted as 5G Std.), WFQ, RR scheduling, PQ, NRFlex, and BestCQI. The assessed performance metrics under varying UE numbers include average delay, net profit, and virtual RB (vRB) utilization. To facilitate reproducibility and enable further research, the implementation of the proposed method is available publicly [49].

Table 6: Flow queueing scheduling of compared approaches.

Compared Approaches	Flow Queue Scheduling
The proposed eSCFS approach	Adaptive Cost-Reward functions
5G/5G-A Std. [2,3]	Packet rate (packet RX/TX)
NRflex [20]	Min delay and Packet rate
5G + PQ [45]	PQ + Slicing
5G + WFQ [41]	WFQ + latency bound
5G + RR [48]	Greedy + RR
5G + BestCQI [49]	BestCQI

In the proposed network model, the 5G/5G-A NR system consists of a two-tier architecture with a total of seven gNBs and a core network. Each gNB allocates 10 MHz of bandwidth to support three NR SCS modes. A single 5G/5G-A Physical System Frame (PSF) is composed of 10 sub-frames, spanning a duration of 10 ms. Regarding the traffic model, three distinct types of flows are considered: uRLLC and emergency (eMERGENCY) flows for eV2X applications, mMTC+ flows for 5G-A IIoT, and enhanced mobile broadband (eMBB+) flows. Flow generation at each UE follows a Pareto distribution, characterized by parameters α_on, α_off, and β. The detailed characteristics of these flows are summarized in Table 7.

Table 7: Simulation parameters.

Compared Approaches	Flow Queue Scheduling
Length of simulation	120 s
gNBs (2-Tier)	7
Frequency Spectrum Bandwidth (MHz)	20 MHz
SCS modes for numerology μ	$\{0, 1, 2\}$
Slot configuration within a subframe	$\{1, 2, 4\}$
Number of RBs per subframe(different SCS modes)	$\mu_0 = 106$, $\mu_1 = 102$, $\mu_2 = 96$
Number of UEs	$\{1000, 1500, 2000, 2500, 3000, 3500, 4000\}$
Max delay bound (ms)	$\mu_0 = 50$ ms, $\mu_1 = 10$ ms, $\mu_2 = 5$ ms
Packet length (Bytes)	512, 1024, 1500 Bytes

In Figs. 7–9, the average vRB access delay among all compared approaches under different numbers of UEs are compared. In Fig. 7 for the highest priority SCS mode, all average delays increase as the number of UEs increases. eSCFS and 5G/5G-A Std. result in competitive higher delay. The reason is that eSCFS aims to yield an access delay less than the delay bound of 5 ms, rather than achieves the minimum access delay. However, PQ and WFQ result in the least delay, because they always schedule the highest priority flow to minimize the access delay while neglecting the bringing reward and the carrying cost. Moreover, NRFlex and BestCQI lead to higher delay, because of concerning a single major factor and neglecting the bringing reward and the carrying cost. Obviously, the proposed eSCFS scheduling algorithm is based on adaptive cost/reward functions with maximizing net-profit, pre-allocating the vRB with the least vRB MX, and the least fragment of available vRBs. Consequently, eSCFS certainly yields the least vRB access delay, while resulting in supreme advantages: the least vRB MX and the least fragmental vRB.

In Fig. 8, for the higher priority SCS mode μ_1, all average delay increases as the number of UEs increasing. NRFlex yields the longest average vRB delay because it considers only the delay metric as the important factor. eSCFS yields the longest delay for SCS mode μ_1, because in eSCFS the highest SCS mode μ_2 always brings the highest reward and adopts the exponential-based cost according to the vRB state. Similarly, PQ yields much higher delay for the higher priority SCS mode μ_1 due to PQ always scheduling the highest priority SCS mode μ_2 firstly. Clearly, RR and WFQ aim at the fair scheduling criteria and thus yield moderate delay.

In Fig. 9, for the least priority SCS mode μ_0, eSCFS yields the least delay, because eSCFS searches available vRB for allocation according to the descending time from the delay bound (i.e., 50 ms) to the current time. However, the other approaches result in competitive high delays, because they adopt PP specified 3 types of RB allocations or random allocation for the lowest priority of the SCS mode μ_0.

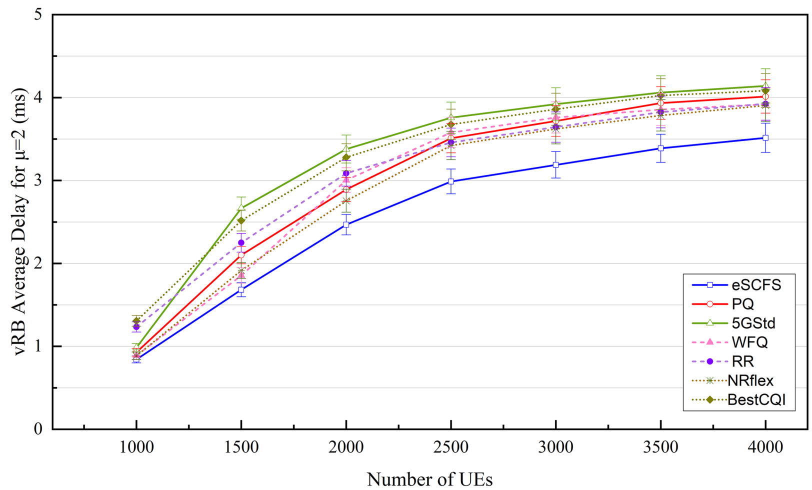

Figure 7: Average delay of the highest priority SCS mode μ_2.

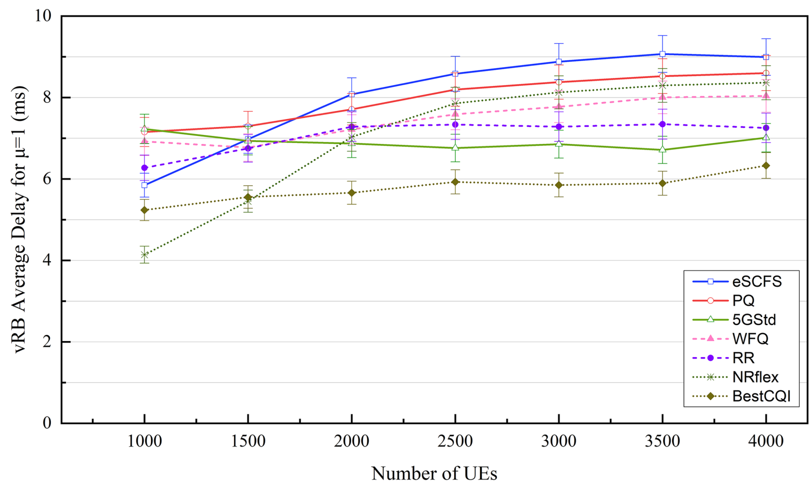

Figure 8: Average delay of the higher priority SCS mode μ_1.

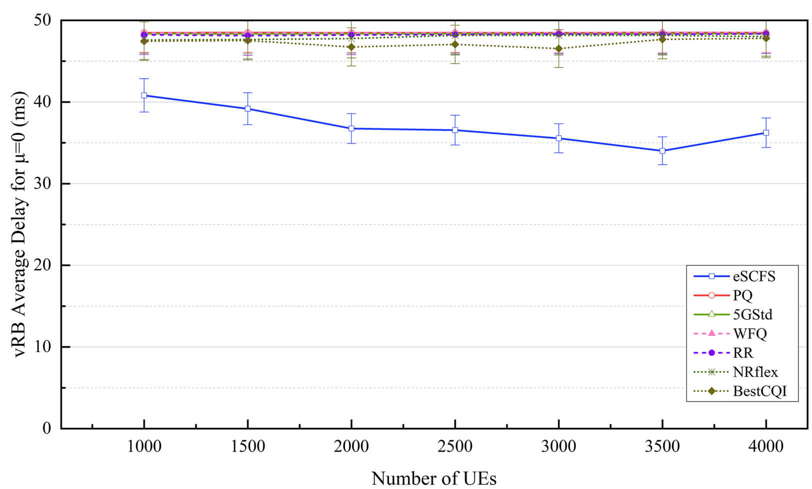

Figure 9: Average delay of the lowest priority SCS mode μ_0.

Figs. 10–12 evaluate average vRB utilizations among all compared approaches. Certainly, lowering the Mutual eXclusion or the fragmental vRBs is equivalent to achieving a higher vRB utilization. In Fig. 10, for the highest priority of the SCS mode μ_2, eSCFS yielding the highest vRB utilization benefits from the adaptive maximum Net-Profit scheduling with adaptive vRB allocation. However, RR and BestCQI lead to the least utilization. RR and BestCQI suffer from fairness scheduling and single concerning CQI factor for the flow scheduling, respectively. Finally, 5G, PQ, and WFQ lead to moderate vRB utilization of the SCS mode μ_2. Specifically, PQ always schedules the highest priority SCS mode μ_2 firstly and neglects the MX effect in vRB allocation.

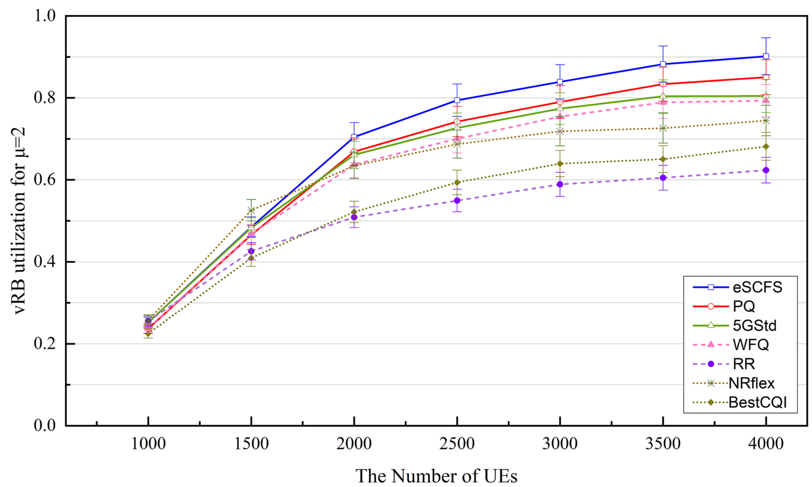

Figure 10: Average vRB utilization of different numbers of UEs of the highest priority SCS modes μ_2.

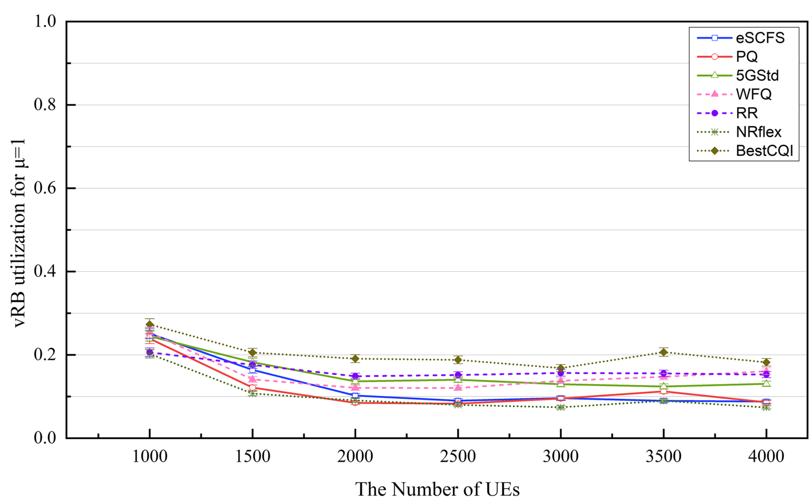

Figure 11: Average vRB utilization of different numbers of UEs of the highest priority SCS modes μ_1.

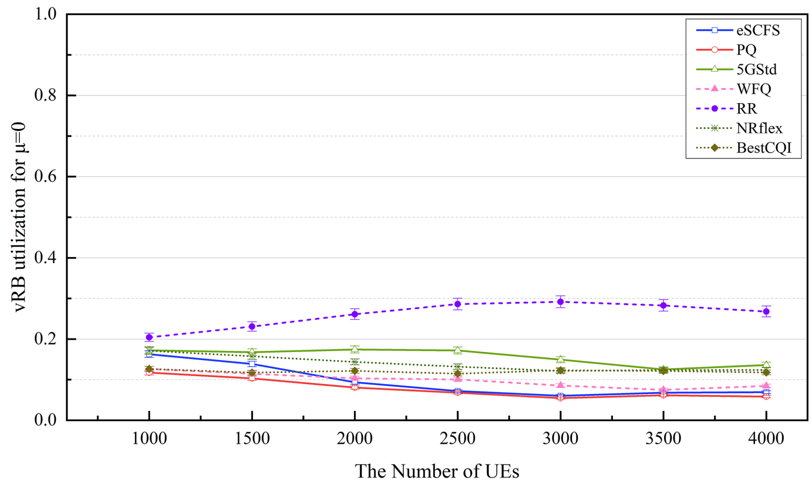

Figure 12: Average vRB utilization of different numbers of UEs of the highest priority SCS modes μ_0.

Fig. 11 evaluates vRB utilization of the high priority of SCS mode μ_1, where 5G std. and PQ yield the least vRB utilization, but RR and BestCQI lead to the highest utilization. Moreover, eSCFS results in low utilization, because the proposed Cost-Reward-based approach efficiently allocates vRB for SCS mode μ_2 but may degrade the vRB utilization of SCS modes μ_1 and μ_0. Furthermore, all the compared approaches neglect the critical problems of MX and fragmental vRB. Typically, for SCS mode μ_1, PQ and Nrflex yield the least vRB utilization. 5G, WFQ, and RR yield moderate vRB utilization for the high priority SCS mode μ_1. Specifically, PQ contributes to the highest priority SCS mode μ_2 only. For SCS mode μ_1, Nrflex yields the least vRB utilization.

Fig. 12 compares the vRB utilization of the lowest priority of the SCS mode μ_0, in which the proposed eSCFS yields the lowest vRB utilization, but 5G and RR lead to the highest vRB utilization. The others lead to competitive moderate vRB utilization. For eSCFS, the lowest priority SCS mode is easily blocked because the carrying cost is higher than the bringing reward, and thus minimizes the utilization. Conversely, RR, BestCQI, Nrflex, and 5G only concern fairness, a single QoS metric of CQI, or flow priority, so they result in the highest or moderate vRB utilization.

Figs. 13–15 evaluate the total bringing reward, total carrying cost, and total net profit, respectively. Clearly, an approach allocating a larger number of vRBs definitely increases the vRB utilization and the carrying cost. Thus, to efficiently allocate vRB while not increasing total carrying cost, but increasing the bringing reward and total net-profit becomes a huge challenge in 5G/5G-A networks. Obviously, different types of flows bring different rewards. As a result, it exhibits a trade-off between increasing the vRB utilization and not increasing the total carrying cost and the total bringing reward.

Fig. 13 evaluates the total bringing reward, where eSCFS outperforms the other approaches in the bringing reward, benefiting from two key mechanisms: 1) the adaptive maximum net-profit scheduling algorithm according to the vRB state and 2) the adaptive vRB allocation with minimizing MX vRBs and fragmented vRBs. PQ and WFQ yield low total bringing reward because of scheduling more flows of SCS mode μ_2 that brings a higher reward. 5G and NRflex yield competitive low bringing reward. Finally, RR and BestCQI result in the lowest reward due to their non-adaptive nature. RR provides fair scheduling regardless of flow type, channel quality, etc. BestCQI's performance is limited by statically using CQI only and neglecting the flow type.

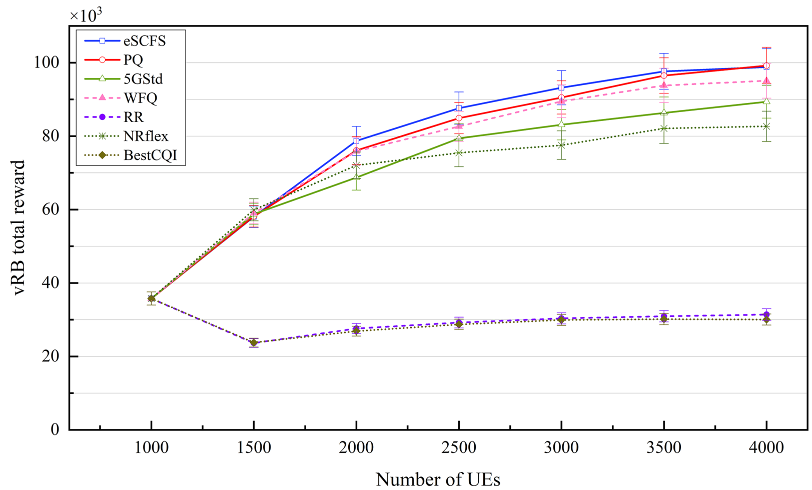

Figure 13: Total bringing reward.

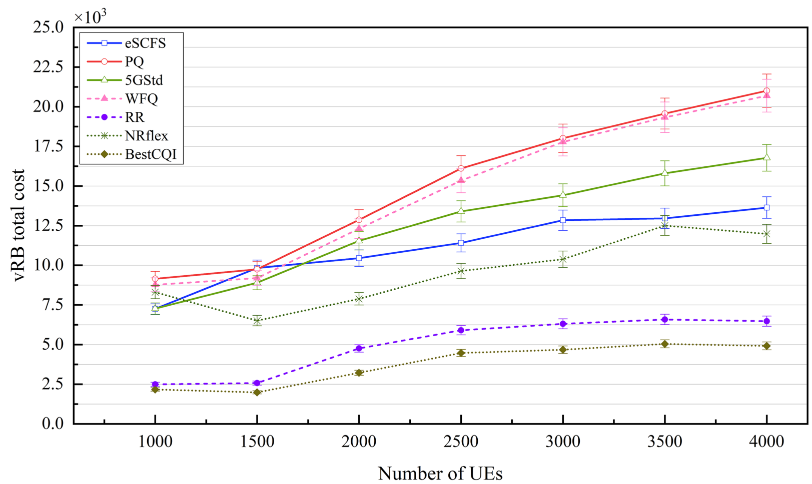

Figure 14: Total carrying cost.

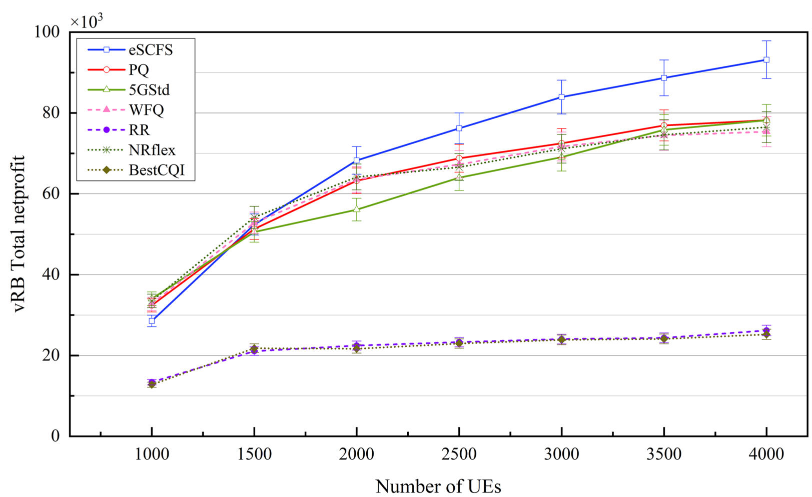

Figure 15: Total net profit.

Fig. 14 evaluates the total carrying costs. PQ and WFQ result in the highest cost due to prioritizing packets in the highest-priority SCS modes. 5G Std. yields a higher total carrying cost. eSCFS results in moderate cost, benefiting from the adaptive cost and reward functions. RR yields much lower cost, and BestCQI yields the least carrying cost because of neglecting several key factors, including the flow type, the vRB state, the MX feature in 5G/6G frequency numerology, etc.

Fig. 15 evaluates the total net-profit, in which eSCFS yields the highest net-profit by using the proposed adaptive exponential cost function according to the vRB state and the extended Sigmoid reward function. RR and Best CQI yield the least net profit because they yield the least total reward. The other approaches (5G Std., PQ, WFQ, and NRflex) result in moderate total net-profit because of neglecting several important mechanisms, including the cost and reward functions, the vRB state, the MX feature of frequency numerology in 5G, etc.

Fig. 16 demonstrates the normalized delay of SCS mode μ_2 of BestCQI as the baseline for clearly demonstrating the overhead of the delay comparison among all approaches. Obviously, the approach yielding the least overhead of delay certainly results in the least processing time even under heavy traffic loading. Consequently, such an approach definitely achieves the highest scalability. In Fig. 16, the normalized delay overhead of 5G Std is always higher than that of BestCQI. That is, 5G Std yields worse overhead of the delay than BestCQI, because 5G Std uses maximum rate-based scheduling. Moreover, the other approaches (except for 5G Std) yield lower normalized delay overhead than that of BestCQI. Especially, the proposed eSCFS approach outperforms the other compared approaches in the normalized delay overhead, because of the maximum net-profit scheduling flow scheduling (according to the vRB state) and the adaptive vRB allocation. Specifically, in eSCFS, the maximum net-profit scheduling contributes to the least overhead of the delay for SCS mode μ_2 and the highest processing scalability.

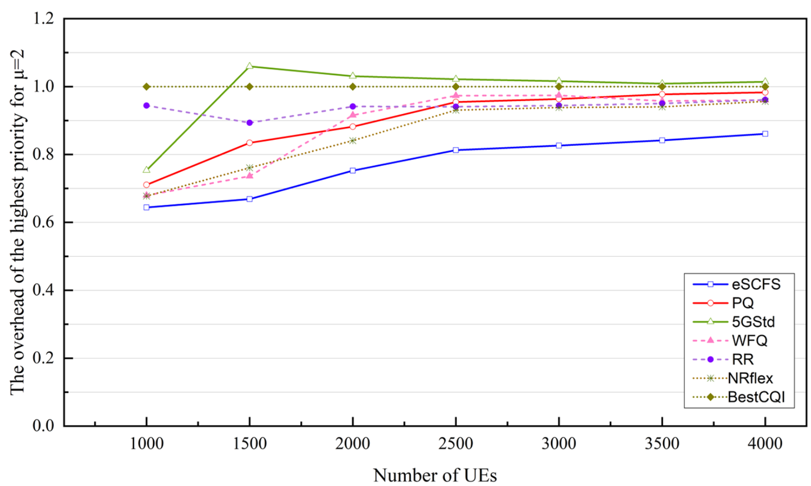

Figure 16: Normalized the overhead of the delay to the baseline BestCQI (SCS mode μ_2).

5 Conclusions and Future Directions

In 5G-A TN and 6G NTN LEO, a key enabling technique is frequency numerology, which defines different slot times for different SCS modes for achieving extremely low delay and ultra-reliable communications. However, such numerology suffers from dynamic, diverse types of flow traffic, a mutual exclusion feature among all vRB resources, and fragmental vRBs. Furthermore, 3GPP specified three types of RB allocations, which clearly suffers from statically pre-configuration BWP. As a result, the vRB allocation efficiency is obviously degraded. Furthermore, for the scheduling, the core mechanism of flow scheduling is to dynamically differentiate the prioritization of flow packet processing according to single or multiple metrics. The critical challenges in flow scheduling and vRB allocation in 5G-A TN and 6G NTN LEO need to be addressed efficiently. Thus, this work proposed an Extended Sigmoid-based Cost-Reward Flow Scheduling (eSCFS) approach and achieved several contributions. First, packets in flow queues are prioritized based on net-profit, with the highest net-profit packet assigned the highest scheduling priority. Second, the analyses and discussions of key factors in cost and reward functions are presented. Third, minimizing the MX and fragmental vRB in 5G-A TN/6G NTN frequency numerology for enhancing spectrum efficiency. Numerical results demonstrate that eSCFS outperforms existing methods in terms of vRB utilization, average delay, total bringing reward, and average net-profit.

3GPP 6G NTN LEO communications specified the frequency numerology using three SCS modes with limited frequency spectrum bandwidth. Thus, the proposed eSCFS approach can be extended to 6G NTN LEO satellites for edge-AI computing. Typically, we have studied and realized the AI Markov Decision Process-based Reinforcement Learning (MDP-RL) for the optimal predictions of flow queue state and vRB state. The MDP state and the action state, according to the 6G NTN LEO network environment, have been defined and analyzed. Several 6G LEO research studies of SDN-based flowing radio RB allocation with deep MDP-RL learning and training have been studied as future work.

Acknowledgement: Not applicable.

Funding Statement: The authors received no specific funding for this study

Author Contributions: The authors confirm contribution to the paper as follows: study conception and design: Wei-Teng Chang and Ben-Jye Chang; data collection: Wei-Teng Chang; analysis and interpretation of results: Wei-Teng Chang and Ben-Jye Chang; draft manuscript preparation: Wei-Teng Chang and Ben-Jye Chang. All authors reviewed and approved the final version of the manuscript.

Availability of Data and Materials: Not applicable.

Ethics Approval: Not applicable.

Conflicts of Interest: The authors declare no conflicts of interest.

List of Abbreviations

3GPP	3rd Generation Partnership Project
5G	5th-Generation Mobile Communication Technology
5G-A	5G-Advanced
5QI	5G QoS Identifier
6G	6th-Generation Mobile Networks
AI	Artificial Intelligence
ALC	Adaptive Wireless Connectivity
AR	Augmented Reality
B5G	Beyond 5G
BWP	Bandwidth Part
CP	Control Plane
DCI	Downlink Control Information
DL	Downlink
EC	Edge Computing
eMBB	enhanced Mobile Broadband
EWFQ/LC	Extended Weighted Fair. Queueing with Latency Constraint

FR1	Frequency Range 1
FR2	Frequency Range 2
eV2X	enhanced Vehicle-to-Everything
gNB	next-generation NodeB
IoT	Internet of Things
KPI	Key Performance Indicators
LEO	Low Earth Orbit Satellite
MCS	Modulation and Coding Scheme
MEC	Mobile Edge Computing
ML	Machine Learning
mMTC	massive Machine-Type Communications
NFV	Network Function Virtualization
NTN	Non-Terrestrial Networks
NR	New Radio
PF	Proportional Fair
PI	Price Index
Pkt	Packet
PQ	Priority Queuing
pRB	physical Resource Block
QoE	Quality of Experience
QoS	Quality of Service
RAN	Radio Access Network
RB	Resource Block
RBG	Resource Block Group
RR	Round Robin
RX	Receive
SCS	Subcarrier Spacing
SDN	Software-Defined Networking
SDVN	Software-Defined Vehicular Networks
SFC	Service Function Chaining
TN	Terrestrial Networks
TX	Transmit
UL	Uplink
UP	User Plane
uRLLC	ultra-Reliable Low-Latency Communications
VCC	Vehicle Cloud Computing
VEC	Vehicle Edge Computing
VR	Virtual Reality
vRB	virtual Resource Block
WFQ	Weighted Fair Queuing
WRR	Weighted Round-Robin

References

1. Khan MU, García-Armada A, Escudero-Garzás JJ. Service-based network dimensioning for 5G networks assisted by real data. IEEE Access. 2020;8:129193–212. doi:10.1109/ACCESS.2020.3009127.
2. 3GPP TS 38.211 V19.1.0. NR; medium access control (MAC) protocol specification. Sophia-Antipolis, France: 3GPP; 2025.
3. 3GPP TS 38.214 V19.1.0. NR; physical layer procedures for data specification. Sophia-Antipolis, France: 3GPP; 2025.

4. Chang BJ, Chang WT. Cost-reward-based carrier aggregation with differentiating network slicing for optimizing radio RB allocation in 5G new radio network. In: 2019 IEEE 10th Annual Information Technology, Electronics and Mobile Communication Conference (IEMCON); 2019 Oct 17–19; Vancouver, BC, Canada. p. 814–20. doi:10.1109/iemcon.2019.8936296.
5. 3GPP TS 23.501 V19.3.0. System architecture for the 5G system (5GS) stage 2. Sophia-Antipolis, France: 3GPP; 2025.
6. 3GPP TS 38.133 V19.1.0. NR; requirements for support of radio resource management. Sophia-Antipolis, France: 3GPP; 2025.
7. Roger S, Botella-Mascarell C, Martín-Sacristán D, García-Roger D, Monserrat JF, Svensson T. Sustainable mobility in B5G/6G: V2X technology trends and use cases. IEEE Open J Veh Technol. 2024;5(9):459–72. doi:10.1109/OJVT.2024.3375451.
8. Gupta M, Jha RK, Jain S. Tactile based intelligence touch technology in IoT configured WCN in B5G/6G—a survey. IEEE Access. 2023;11(6):30639–89. doi:10.1109/ACCESS.2022.3148473.
9. Pivoto DGS, Rezende TT, Facina MSP, Moreira R, de Oliveira Silva F, Cardoso KV, et al. A detailed relevance analysis of enabling technologies for 6G architectures. IEEE Access. 2023;11:89644–84. doi:10.1109/ACCESS.2023.3301811.
10. Shafi M, Jha RK, Jain S. 6G: technology evolution in future wireless networks. IEEE Access. 2024;12:57548–73. doi:10.1109/ACCESS.2024.3385230.
11. Yılmaz SS, Özbek B. Massive MIMO-NOMA based MEC in task offloading for delay minimization. IEEE Access. 2023;11:162–70. doi:10.1109/ACCESS.2022.3232731.
12. Chang BJ, Hung W, Lin Y, Chang WT. Dynamic keeping reserved resource probability with slicing flow steering in 5G sidelink SPS for platooning ADAS and autonomous self driving. In: 2020 International Automatic Control Conference (CACS); 2020 Nov 4–7; Hsinchu, Taiwan. p. 1–6. doi:10.1109/CACS50047.2020.9289794.
13. Rafid M, Ghafoor H, Koo I. An SVM-based optimal-controller selection and path selection protocol for heterogeneous communications in SDVNs. IEEE Trans Intell Transp Syst. 2024;25(5):3828–42. doi:10.1109/TITS.2023.3326651.
14. Ammar S, Pong Lau C, Shihada B. An in-depth survey on virtualization technologies in 6G integrated terrestrial and non-terrestrial networks. IEEE Open J Commun Soc. 2024;5(6):3690–734. doi:10.1109/OJCOMS.2024.3414622.
15. Zheng G, Wang N, Qian P, Griffin D, Tafazolli RR. SDN-based service function chaining in integrated terrestrial and LEO satellite-based space Internet. IEEE J Sel Areas Commun. 2025;43(2):537–50. doi:10.1109/JSAC.2025.3528807.
16. Barakabitze AA, Mkwawa IH, Hines A, Walshe R. QoE-aware dynamic resource management in future softwarized and virtualized networks. IEEE Access. 2023;11:93310–30. doi:10.1109/ACCESS.2023.3309599.
17. Mosahebfard M, Vardakas JS, Verikoukis C. Modelling the admission ratio in NFV-based converged optical-wireless 5G networks. IEEE Trans Veh Technol. 2021;70(11):12024–38. doi:10.1109/TVT.2021.3113838.
18. Chen R, Zhao J. Scalable and flexible traffic steering for service function chains. IEEE Trans Netw Serv Manag. 2022;19(3):2048–62. doi:10.1109/TNSM.2022.3143139.
19. Habibi MA, Yousaf FZ, Schotten HD. Mapping the VNFs and VLs of a RAN slice onto intelligent PoPs in beyond 5G mobile networks. IEEE Open J Commun Soc. 2022;3:670–704. doi:10.1109/OJCOMS.2022.3165000.
20. Boutiba K, Ksentini A, Brik B, Challal Y, Balla A. NRflex: enforcing network slicing in 5G new radio. Comput Commun. 2022;181(6):284–92. doi:10.1016/j.comcom.2021.09.034.
21. Abedin SF, Mahmood A, Tran NH, Han Z, Gidlund M. Elastic O-RAN slicing for industrial monitoring and control: a distributed matching game and deep reinforcement learning approach. IEEE Trans Veh Technol. 2022;71(10):10808–22. doi:10.1109/TVT.2022.3188217.
22. Alsenwi M, Tran NH, Bennis M, Pandey SR, Bairagi AK, Hong CS. Intelligent resource slicing for eMBB and URLLC coexistence in 5G and beyond: a deep reinforcement learning based approach. IEEE Trans Wirel Commun. 2021;20(7):4585–600. doi:10.1109/TWC.2021.3060514.

23. Waheed A, Ali Shah M, Mohsin SM, Khan A, Maple C, Aslam S, et al. A comprehensive review of computing paradigms, enabling computation offloading and task execution in vehicular networks. IEEE Access. 2022;10:3580–600. doi:10.1109/ACCESS.2021.3138219.
24. Olariu S. A survey of vehicular cloud research: trends, applications and challenges. IEEE Trans Intell Transp Syst. 2020;21(6):2648–63. doi:10.1109/TITS.2019.2959743.
25. Kiri Taksande P, Jha P, Karandikar A, Chaporkar P. Open5G: a software-defined networking protocol for 5G multi-RAT wireless networks. In: 2020 IEEE Wireless Communications and Networking Conference Workshops (WCNCW); 2020 Apr 6–9; Seoul, Republic of Korea. p. 1–6. doi:10.1109/WCNCW48565.2020.9124815.
26. Maity I, Dhiman R, Misra S. MobiPlace: mobility-aware controller placement in software-defined vehicular networks. IEEE Trans Veh Technol. 2021;70(1):957–66. doi:10.1109/TVT.2021.3049678.
27. Leyva-Mayorga I, Soret B, Popovski P. Inter-plane inter-satellite connectivity in dense LEO constellations. IEEE Trans Wirel Commun. 2021;20(6):3430–43. doi:10.1109/TWC.2021.3050335.
28. Garcia MHC, Molina-Galan A, Boban M, Gozalvez J, Coll-Perales B, Şahin T, et al. A tutorial on 5G NR V2X communications. IEEE Commun Surv Tutor. 2021;23(3):1972–2026. doi:10.1109/COMST.2021.3057017.
29. 3GPP TS 38.101-5 V19.2.0. NR; user equipment (UE) radio transmission and reception, Part 5: satellite access radio frequency (RF) and performance requirements. Sophia-Antipolis, France: 3GPP; 2025.
30. 3GPP TS 22.261 V20.4.0. Technical specification group services and system aspects; service requirements for the 5G system, Stage 1. Sophia-Antipolis, France: 3GPP; 2025.
31. Tataria H, Shafi M, Molisch AF, Dohler M, Sjöland H, Tufvesson F. 6G wireless systems: vision, requirements, challenges, insights, and opportunities. Proc IEEE. 2021;109(7):1166–99. doi:10.1109/JPROC.2021.3061701.
32. Hossain A, Ansari N. 5G multi-band numerology-based TDD RAN slicing for throughput and latency sensitive services. IEEE Trans Mob Comput. 2023;22(3):1263–74. doi:10.1109/TMC.2021.3106323.
33. Chang WT, Chang BJ. Dynamic extended sigmoid-based scheduling with virtualized RB allocation for maximizing frequency numerology efficiency in 5G/B5G NR networks. Comput Netw. 2023;237(1):110063. doi:10.1016/j.comnet.2023.110063.
34. Chang WT, Chang BJ. Adaptive cost-reward scheduling for optimizing radio utilization and NR numerology efficiency in B5G new radio networking. In: Advanced information networking and applications. Cham, Switzerland: Springer; 2024. p. 129–39. doi:10.1007/978-3-031-57840-3_12.
35. Lucas-Estañ MC, Coll-Perales B, Shimizu T, Gozalvez J, Higuchi T, Avedisov S, et al. An analytical latency model and evaluation of the capacity of 5G NR to support V2X services using V2N2V communications. IEEE Trans Veh Technol. 2023;72(2):2293–306. doi:10.1109/TVT.2022.3208306.
36. 3GPP TS 38.300 V18.6.0. NR; NR and NG-RAN overall description stage 2. Sophia-Antipolis, France: 3GPP; 2025.
37. Saad J, Yassin M, Costanzo S, Khawam K. Novel BWP schemes for multi-numerology and multi-slice radio access networks. In: 2024 IEEE Wireless Communications and Networking Conference (WCNC); 2024 Apr 21–24; Dubai, United Arab Emirates. p. 161–6. doi:10.1109/WCNC57260.2024.10571292.
38. Liu X, Zhang X, Zhang L, Xiao P, Wei J, Zhang H, et al. PAPR reduction using iterative clipping/filtering and ADMM approaches for OFDM-based mixed-numerology systems. IEEE Trans Wirel Commun. 2020;19(4):2586–600. doi:10.1109/TWC.2020.2966600.
39. Jeon J. NR wide bandwidth operations. IEEE Commun Mag. 2018;56(3):42–6. doi:10.1109/MCOM.2018.1700736.
40. Li YR, Chen M, Xu J, Tian L, Huang K. Power saving techniques for 5G and beyond. IEEE Access. 2020;8:108675–90. doi:10.1109/ACCESS.2020.3001180.
41. Seah WKG, Lee CH, Lin YD, Lai YC. Combined communication and computing resource scheduling in sliced 5G multi-access edge computing systems. IEEE Trans Veh Technol. 2022;71(3):3144–54. doi:10.1109/TVT.2021.3139026.
42. Priyadarshini PR, Bapat J, Mishra A. Channel and delay weighted response ratio scheduler for 5G and beyond systems. IEEE Commun Lett. 2024;28(7):1658–62. doi:10.1109/LCOMM.2024.3403899.
43. Akudo Nwogu O, Diaz G, Abdennebi M. Differential traffic QoS scheduling for 5G/6G fronthaul networks. In: 2021 31st International Telecommunication Networks and Applications Conference (ITNAC); 2021 Nov 24–26; Sydney, NSW, Australia. p. 113–20. doi:10.1109/ITNAC53136.2021.9652162.

44. Weerasinghe TN, Casares-Giner V, Balapuwaduge IAM, Li FY. Priority enabled grant-free access with dynamic slot allocation for heterogeneous mMTC traffic in 5G NR networks. IEEE Trans Commun. 2021;69(5):3192–206. doi:10.1109/TCOMM.2021.3053990.
45. Ivanova D, Markova E, Moltchanov D, Pirmagomedov R, Koucheryavy Y, Samouylov K. Performance of priority-based traffic coexistence strategies in 5G mmWave industrial deployments. IEEE Access. 2022;10(12):9241–56. doi:10.1109/ACCESS.2022.3143583.
46. Li L, Shao W, Zhou X. A flexible scheduling algorithm for the 5th-generation networks. Intell Converged Netw. 2021;2(2):101–7. doi:10.23919/ICN.2020.0017.
47. Elamaran E, Sudhakar B. Greedy based round robin scheduling solution for data traffic management in 5G. In: 2019 International Conference on Smart Systems and Inventive Technology (ICSSIT); 2019 Nov 27–29; Tirunelveli, India. 2020. p. 773–9. doi:10.1109/ICSSIT46314.2019.8987875.
48. Baheti PK, Khunteta A. Priority-based resource scheduling for smart city M2M communication in 5G networks. In: 2023 3rd International Conference on Mobile Networks and Wireless Communications (ICMNWC); 2023 Dec 4–5; Tumkur, India. 2024. p. 1–6. doi:10.1109/ICMNWC60182.2023.10435821.
49. Chang W-T. eSCFS approach, NewRadio-scheduling-research. GitHub repository, 2025 [Internet]. [cited 2026 Jan 10]. Available from: https://github.com/WT-Chung/NewRadio-Scheduling-Research/tree/main/eSCFS_Approach.